

1                   **Subduction initiation at the corner of small oceanic basin**

2                   **Miao Dong<sup>1,2\*</sup>, Tianyao Hao<sup>1,2\*</sup>, Yue Li<sup>1,2</sup>, Jian Zhang<sup>2</sup>, and Gui Fang<sup>3</sup>**

3                   <sup>1</sup>Key Laboratory of Petroleum Resource Research, Institute of Geology and Geophysics, Chinese  
4                   Academy of Sciences, Beijing 100029, China

5                   <sup>2</sup>University of Chinese Academy of Sciences, Beijing 100049, China

6                   <sup>3</sup>PetroChina Hangzhou Research Institute of Geology, Hangzhou 310023, China

7                   Corresponding author: Miao Dong ([dongmiao@mail.iggcas.ac.cn](mailto:dongmiao@mail.iggcas.ac.cn))

8                                   Tianyao Hao ([tyhao@mail.iggcas.ac.cn](mailto:tyhao@mail.iggcas.ac.cn))

9                   **Key Points:**

- 10                   • In small ocean basins subduction initiates at the apex of the corner, regardless of its size  
11                   or angle at the corner.
- 12                   • The smaller the angle of the corner in the oceanic basin, the more likely subduction is to  
13                   initiate.
- 14                   • An angle at the corner greater than 120 degrees is less likely to lead to the subduction  
15                   initiation.

## 16 **Abstract**

17 In Southeast Asia, emerging subduction zones often appear to begin at the corners of small  
18 oceanic basins, which have a triangular-indenter continent–ocean boundary geometry. To  
19 investigate the influence of a triangular indenter on subduction initiation, we performed a series  
20 of three-dimensional numerical simulations with varying indenter angles and base lengths. The  
21 results show that the apex of the indenter constitutes the initial location of subduction,  
22 irrespective of the angle or the extent of the indenter. Smaller angle indenters are more likely to  
23 facilitate subduction initiation. At the same time, wide acute angle indenters are difficult to form.  
24 Our findings suggest that triangular indenter structures may facilitate subduction initiation in  
25 smaller basins; however, the role such indenters in subduction initiation is limited in larger  
26 basins. Our results emphasize the importance of accounting for the three-dimensional geometry  
27 of a subduction zone when examining its subduction dynamics and geological features.

## 28 **Plain Language Summary**

29 In Southeast Asia, new subduction zones near small ocean areas and near locations prone to  
30 subduction have a unique and common feature—subduction starts at triangular indenter–shaped  
31 continent–ocean boundaries. To fully understand how these triangular indenter shapes affect the  
32 initiation of subduction, we employed advanced computer simulations. We varied the angles and  
33 lengths of the indenters in our models. We discovered that, no matter the size of the indenter,  
34 subduction began at the apex of the indenter. Interestingly, smaller indenters are especially good  
35 at initiating subduction. However, forming a wide indenter with small angles in nature appears to  
36 be very difficult. This study indicates that the indenter shape helps subduction start in small  
37 ocean areas but is not as important in larger ocean areas. This insight helps us better understand  
38 how subduction works in different locations on the Earth.

## 39 **1 Introduction**

40 Plate tectonic activity is an essential prerequisite for Earth habitability and sets Earth  
41 apart from other planets (Korenaga, 2012). As the foundation of plate tectonics, understanding  
42 the initiation of subduction remains a significant challenge and frontier in the field of Earth  
43 science (Toth and Gurnis, 1998; Gurnis, 2004; Stern, 2004; Korenaga, 2013; Stern and Gerya,  
44 2018). However, one of the most notable difficulties in subduction initiation research is the lack  
45 of “direct observations” (Mueller and Phillips, 1991). Regions that are actively undergoing  
46 subduction initiation, such as Puysegur, can very rarely be directly observed (Gurnis et al., 2004;  
47 Shuck et al., 2022). Therefore, the subduction initiation process is usually studied using various  
48 techniques such as numerical simulations, physical simulations, and petrology (McKenzie, 1977;  
49 Bercovici, 2003; Niu et al., 2003; Agard et al., 2007, 2016; Ishizuka et al., 2011; Gerya et al.,  
50 2015; Maunder et al., 2020; Zhou et al., 2020; Dong et al., 2022) because mature subduction  
51 zones have undergone long periods of tectonic evolution, resulting in the disappearance of most  
52 structural features dating from the initial stage of subduction. Therefore, it is important to  
53 observe and study subduction initiation in areas where subduction initiation is either in progress  
54 or has recently been completed (Hall, 2019; Shuck et al., 2022).

55 Southeast Asia is home to several small oceanic basins and subduction zones that are  
56 relatively young (Figure 1a; Hall, 1996; 2012; Hall and Spakman, 2015; Lai et al., 2021; Li et  
57 al., 2023). Examples include the Cotabato and Sulawesi subduction zones, which were initiated  
58 during the Pliocene or Late Miocene (Silver et al., 1983; Kopp et al., 1999; Schlüter et al., 2001)

59 and have subduction slabs with a maximum depth in the middle of the trench and a gradual  
60 decrease in length along both sides (Figure 1c and 1d). Other regions have ongoing subduction  
61 initiation, such as the Tolo Trough (Figure 1b), where a portion of the continental crust is  
62 migrating over the oceanic crust of the Northern Banda Sea (Silver et al., 1983; Hall, 2019;  
63 Husson et al., 2022). In areas such as the Sula Deep (Figure 1b), which has abnormally deep  
64 water and steep terrain, subduction initiation seems probable in the future (Hall, 2019). Despite  
65 differences in their subduction initiation stages, these regions share similar structural  
66 characteristics, with oceanic lithosphere subducting beneath either a relic arc or a continental  
67 fragment. Moreover, and more importantly, subduction initiation, either ongoing or imminent, is  
68 consistently located in the corners of these oceanic basins (i.e., there is a triangular indenter).

69 Subduction initiation is a complex process that is affected by multiple factors, including  
70 the density differences between the plates, thermal structure, and weak zones (Niu et al., 2003;  
71 Nikolaeva et al., 2010; Leng and Gurnis, 2015; Zhou et al., 2020). For example, Nikolaeva et al.  
72 (2010, 2011) conducted numerical simulations of subduction initiation in a passive continental  
73 margin and proposed that subduction initiation is facilitated by a thick crust and a thin, hot  
74 lithosphere. Similarly, Leng and Gurnis (2015) concluded that, based on numerical simulations,  
75 subduction initiation is easier in arc regions than in passive margins. The overriding plates in the  
76 small, mostly island arc, subduction zones in Southeast Asia are consistent with the results of  
77 these studies. However, these studies were based on two-dimensional (2D) numerical models.  
78 Some lateral structural geometry changes affecting subduction initiation may require three-  
79 dimensional (3D) numerical models. With the rapid development of computing power, more 3D  
80 models are now being used to study subduction initiation (Gerya et al., 2015; Zhou et al., 2018;  
81 2020; Almeida et al., 2022; Riel et al., 2023).

82 Marques et al. (2014) used three 3D models to investigate subduction initiation at a  
83 passive continental margin (where the angle is zero between the trace of the curved section of the  
84 margin and the  $z$ -axis of the model), as well as other models at different angles to the  $z$ -axis.  
85 Their results showed that a straight passive margin is more susceptible to subduction initiation  
86 than a curved passive margin. However, these models did not incorporate geometric shapes such  
87 as a “triangular indenter,” which refers to a specific location where the oceanic plate boundary  
88 geometry exhibits a change in direction, causing it to zigzag toward the continent and form an  
89 angle. Significantly, the small oceanic basins in Southeast Asia differ significantly from the long,  
90 generally straight margins of the Atlantic. In Southeast Asia, the continent–ocean boundaries are  
91 typically much narrower, formed more quickly, and are much steeper (Hall, 2019). Currently,  
92 there are no numerical models available to validate the observed subduction-prone corners in  
93 Southeast Asia.

## 94 **2 Model setup**

95 We employed the massively parallel finite element code ASPECT (Bangerth et al., 2020;  
96 Heister et al., 2017; Kronbichler et al., 2012) to construct and execute our 3D numerical  
97 geodynamic model (Figure 2a). The left side of the model represents the oceanic plate, composed  
98 of the oceanic crust (10-km thick) and the suboceanic lithospheric mantle. The right side of the  
99 model represents the overriding plate, comprising the upper crust (25-km thick), lower crust (15-  
100 km thick), and lithospheric mantle (40-km thick). This configuration creates a substantial density  
101 contrast between the overriding plate and the oceanic plate (Figure 2b). We adopted this specific  
102 setup for the overriding plate model based on previous studies (Nikolaeva et al., 2010; Marques

103 et al., 2014), allowing the model to achieve completion within a short time. Detailed information  
104 concerning the initial model design, equations, and parameters can be found in the Supporting  
105 Information Text S1.

106 A 10-km-thick weak zone between the oceanic plate and the overriding plate is included  
107 in our model to ensure that subduction initiation can be completed. Typically, the boundary  
108 between the oceanic plate and the passive continental margin is not vertical in the  $z$ -direction and  
109 part of the oceanic plate extends below the continental plate (Nikolaeva et al. 2010, 2011;  
110 Marques et al., 2013; 2014). Nevertheless, for the small basins in Southeast Asia, the overriding  
111 plates may closely resemble the lithosphere of relic arcs. Therefore, we adopted a similar  
112 approach to that of Leng and Gurnis (2015) by vertically dividing the plates according to their  
113 weak zones; this allowed us to isolate just the impact of the indenter geometry on subduction  
114 initiation.

115 In our models, the geometry of the indenter is defined by the angle  $\alpha$  and width  $D$  of the  
116 base extent of the corner (Figure 2c). Model 0 (a straight ocean–continent boundary, invariant in  
117 the  $z$ -direction) serves as the reference model to evaluate the influence of the indenter. Models 1,  
118 2, and 3 have a width  $D$  of 200 km, with  $\alpha$  values of  $120^\circ$ ,  $90^\circ$ , and  $60^\circ$ , respectively. Models 4,  
119 5, and 6 have a width  $D$  of 115.4 km, with  $\alpha$  values of  $120^\circ$ ,  $90^\circ$ , and  $60^\circ$ , respectively. Model 7  
120 shares the same apex positions as Models 1 and 5, with an  $\alpha$  value of  $60^\circ$ . Models 8, 9, and 10  
121 have a width  $D$  of 346.4 km, with  $\alpha$  values of  $120^\circ$ ,  $90^\circ$ , and  $60^\circ$ , respectively.

### 122 **3 Results**

123 In this study, we designated the time at which the sinking oceanic slab reaches a depth of  
124 200 km as the completion time of subduction initiation (Figures 3a and S1), serving as a metric  
125 to evaluate the level of difficulty for each model to achieve subduction initiation. Because the  
126 temporal resolution of our model output is 0.1-Myr intervals, there may be an associated error of  
127  $\pm 0.1$  Myr in the recorded time (Table 1).

128 In comparison to the reference model (Model 0), characterized by a straight ocean–  
129 continent boundary, the majority of the models featuring an indenter structure demonstrated  
130 accelerated subduction initiation. Only Model 1 exhibited a longer initiation period than the  
131 reference model. Note that, because of the marginal error of 0.1 Myr, the subduction initiation  
132 times in Models 4 and 8 can be approximated as being similar to those of the reference model.  
133 Interestingly, Models 1, 4, and 8 share the same angle of  $120^\circ$ .

134 In the simulations involving Models 1, 2, and 3, all featuring an indenter structure with a  
135 consistent base extent of 200 km, we observed that a larger angle ( $\alpha$ ) was correlated with  
136 extended durations for completing subduction initiation. This trend was also evident in other  
137 models with varying  $D$  values, such as Models 4, 5, and 6, as well as Models 8, 9, and 10.  
138 Accordingly, we conclude that, for indenter structures sharing the same base extent, a smaller  
139 angle tends to lead to quicker subduction initiation.

140 Despite these results, no consistent pattern emerged for models with the same angle but  
141 differing base lengths. For example, when considering an angle of  $120^\circ$ , Model 1, with  $D = 200$   
142 km, required 5.0 Myr to achieve initial subduction. In contrast, Model 4, with a smaller indenter,  
143 and Model 8, with a wider indenter, both exhibited shorter subduction initiation times.

144 The results for models featuring a  $90^\circ$  angle diverged from those with a  $120^\circ$  angle.  
145 Notably, Model 2, with a indenter base extent of 200 km, exhibited a higher probability of

146 subduction initiation than both the narrower indenter (Model 5) and the wider indenter (Model 9),  
147 which required more time to complete initial subduction than Model 2. Nevertheless, all models  
148 with a  $90^\circ$  angle accomplished initial subduction more rapidly than Model 0.

149 In the case of models with an angle of  $60^\circ$ , analogous to those with an angle of  $90^\circ$ , the  
150 model (Model 3) with  $D = 200$  km completed subduction initiation faster, whereas both of the  
151 narrower indenters (Models 6 and 7) and the wider indenter (Model 10) exhibited lengthier  
152 subduction initiation times. However, the time difference was not as pronounced as observed in  
153 models with a  $90^\circ$  angle. Considering the potential error of 0.1 Myr, Models 3 and 10 are  
154 reasonably similar. Consequently, the relationship between the time required for initial  
155 subduction completion and the base extent  $D$  is not linearly dependent given a constant indenter  
156 angle.

157 Analyzing models sharing the same apex position ( $h$ ), yet varying in angle, we reached  
158 similar conclusions. For example, Models 1, 5, and 7, possessing identical apex positions,  
159 demonstrated that a smaller angle leads to a briefer duration for initial subduction. However,  
160 within the context of models with the same angle, the discrepancy in the subduction initiation  
161 time arising from different  $h$  values did not adhere to a linear pattern.

## 162 **4 Discussion**

### 163 4.1 Influence of the 3D indenter geometry on subduction initiation

164 In a 3D model, the magnitude of the vertical downward force (the  $y$ -component) can be  
165 amplified or diminished given the presence of a horizontal component (the  $z$ -component). This  
166 component, a representation of the third spatial dimension lacking in a 2D model, influences the  
167 distribution of forces within the 3D framework.

168 For the first few timesteps (less than 1 Myr), the continental plate undergoes rapid  
169 vertical movement to reach isostatic equilibrium (Figures 4b, S2b, and S3b). Subsequently, the  
170 primary driving force, originating from the density contrast between the oceanic and continental  
171 plates (Figure 2b), causes the overriding plate to overthrust onto the oceanic plate, inducing  
172 downward bending of the latter. Particularly at the apex of the indenter, a focusing effect  
173 facilitates the dipping of the indenter. As subduction initiation progresses, the leading edge  
174 increases its buoyancy contrast with the surrounding mantle, intensifying the bending and the  
175 downward pull of the plate.

176 As subduction initiation progresses, the indenter area on the surface gradually decreases  
177 (Figures 4b, S2b, and S3b). However, the extent of this reduction varies among the models with  
178 different angles. Models with smaller initial angles experience greater reductions in the extent of  
179 the indenter ( $D$ ) and in the reduction of  $h$  ( $\Delta h$ ). In models with large angle indenters, the force  
180 component in the  $z$ -direction is smaller than that in the  $x$ -direction. While the apex position of the  
181 indenter has a force in the  $z$ -direction on both sides that pushes the oceanic plate downward, this  
182 force is too small to change the deformation of the overriding plate in the indenter. As a result,  
183 the change in the length  $h$  is relatively small and the overriding plate moves toward the oceanic  
184 plate along the  $x$ -direction, with the continent–ocean boundary shape remaining largely  
185 unchanged (Figure 4b). Therefore, large-angle indenters have little effect on subduction initiation  
186 because they lose the focusing effect of the indenter as nearly the entire margin geometry  
187 becomes triangular. According to our numerical simulations, the indenter does not promote  
188 subduction initiation when the angle of the indenter exceeds  $120^\circ$ .

189 In the case of a small angle indenter, the component of the force in the  $z$ -direction is  
190 sufficiently large to induce deformation of the overriding plate. Consequently, the oceanic  
191 lithosphere at the apex of the indenter is compressed by the overriding plate on both sides,  
192 causing the apex position of the indenter to gradually close. This leads to the oceanic plate at the  
193 apex sinking rapidly into the asthenosphere. As the plate reaches asthenospheric depths, the  
194 buoyancy contrast and viscosity contrast between the subducting plate and the surrounding  
195 mantle increase. Consequently, slab pull becomes increasingly significant. Therefore, the sooner  
196 the oceanic plate at the indenter enters the asthenosphere, the earlier the entire subduction system  
197 will form (Figures 3a and S1).

#### 198 4.2 Initial subduction starts at the indenter point

199 In all models, the apex position of the indenter is the site at which the model plate first  
200 begins to bend downward, irrespective of the angle or extent of the indenter. The subducting slab  
201 reaches a depth of 200 km first at the midsection of the plate (as shown in Figure 3b). This is  
202 consistent with the conditions observed in the Celebes Sea, where the subducted slab has reached  
203 the deepest point at middle of the trench both in the Cotabato and North Sulawesi subduction  
204 zones.

205 The current plan views of the subduction zones appear to be relatively flat without  
206 prominent indenters (gray areas in Figure 1c). However, this does not indicate the shape of the  
207 plate prior to subduction. On the basis of the Slab2.0 model, we can calculate the length of the  
208 subducted slab along the trench-normal direction. Then, we can reconstruct the slab to its pre-  
209 subduction shape (Figure 1d). We can see that there is a triangle indenter at the front end of the  
210 reconstructed plate for both Cotabato and North Sulawesi (red areas in Figure 1c). The longest  
211 slab, corresponding to the location where the subduction initiation first starts, is the apex of the  
212 indenter. This is consistent with our simulation results, which show that subduction initiation  
213 starts at the apex of the indenter.

214 Our modeling results also correspond to the conditions observed in the North Banda Sea.  
215 The region's deepest points correspond to indenter apex positions (Figure 1b). The northeastern  
216 indenter of this region (the Sula Deep) exhibits depths exceeding 5800 m, characterized by slope  
217 gradients of up to  $13^\circ$  (Hall, 2019). These gradients are likely related to slab pull at depth  
218 resulting from roll back in the Banda Sea (Husson et al., 2022). The Tolo Trough, located at the  
219 western edge, exhibits average slope gradients of  $7\text{--}8^\circ$  near its deepest segment. Rudyawan and  
220 Hall (2012) have documented thrusting in this region, consistent with downslope movement of a  
221 thrust sheet and the displacement of continental crust onto the North Banda Sea oceanic crust.

222 Both numerical simulations and geological observations consistently indicate that  
223 subduction initiation predominantly takes place at the indenter apex, irrespective of the indenter  
224 angle or extent. This phenomenon arises from the inherent property of the indenter geometry,  
225 which concentrates stress at its vertices, particularly during the initial stage of subduction  
226 (Figures 4a, S2a, and S3a). The apexes of indenters, where stress concentrates, are more  
227 susceptible to deformation than other areas. In addition, the stress concentration in the corner of  
228 an indenter with a smaller angle is greater; this is the primary reason why the corner model with  
229 a smaller angle is more likely to speed up subduction initiation.

230 Although an acute angle indenter geometry can easily trigger subduction initiation, this  
231 structure is unstable because it is easily compressed by both sides of the plate (Figure 4).

232 Consequently, forming a wide range of such sharp indenters in actual geological cases is  
233 challenging. If these structures were to form during oceanic plate development, before reaching  
234 significant size, intense stresses would rapidly compress the indenter area, particularly at the  
235 apex, potentially leading to subduction. As a result, such large acute angle indenter structures are  
236 not observed on the Earth's surface at present.

237 The promotion of subduction initiation by an indenter primarily relies on the negative  
238 buoyancy of the plate bending downward at the apex position. In smaller basins (hundreds of  
239 kilometers in size), inverting the short margin necessitates a smaller force, allowing a small acute  
240 or right-angled indenter to facilitate subduction initiation. However, in larger basins (several  
241 thousands of kilometers in scale), inverting the entire long margin demands a larger force,  
242 indicating the need for a large acute angular indenter. Unfortunately, such a large indenter  
243 formation is improbable. Therefore, while the triangular indenter structure may facilitate  
244 subduction initiation in smaller basins, its role in larger basins is limited.

#### 245 4.3 Model limitations

246 In this study, all of the simulations accounted for the weak zone at the ocean–continent  
247 boundary, with different indenter geometries corresponding to various weak zone configurations.  
248 However, these models are idealized. In geological settings, the strength of the ocean–continent  
249 boundary relies on inherited structures and the degree of serpentinization, which may not  
250 uniformly exhibit low strength across the entire boundary. Consequently, subduction initiation is  
251 more likely to occur where weak strength areas are present (Zhou et al., 2020).

252 While our models were designed to simulate spontaneous subduction, it is crucial to  
253 acknowledge that small basins, often situated amidst numerous active plates, can experience  
254 influences from surrounding plate activities during subduction initiation (Dong et al., 2022).  
255 Quantifying external forces acting in different directions within a 3D model is complex.  
256 Therefore, we intentionally omitted external forcing, focusing solely on assessing the impact of  
257 the indenter geometry on subduction. Further research involving more complex structures and  
258 boundary conditions closer to those of natural subduction zones is necessary to enable a  
259 comprehensive understanding of subduction initiation dynamics.

### 260 5 Conclusions

261 In this study, we simulated a series of numerical models to investigate the relationship  
262 between the triangular indenter geometry and subduction initiation. The results of the study  
263 suggest the following conclusions.

264 (1) In small oceanic basins, subduction initiates at the apex of the indenter, regardless of  
265 its size or angle.

266 (2) A small angle indenter in an oceanic basin is favorable to subduction initiation.

267 (3) An indenter with an angle of more than  $120^\circ$  does not facilitate subduction initiation  
268 and may instead hinder it.

### 269 Acknowledgments

270 The authors thank Nicolas Riel and Robert Hall for reviewing this manuscript, as well as Lucy  
271 Flesch for her efficient editorial handling. This work was supported by the NSFC (42276072,

272 91858212, 42176052), Strategic Priority Research Program of the CAS (XDB42020104),  
 273 International Partnership Program of the Bureau of International Cooperation of the CAS  
 274 (132A11KYSB20180020). We thank the Computational Infrastructure for Geodynamics  
 275 (geodynamics.org), which is funded by the National Science Foundation under award EAR-  
 276 0949446 and EAR-1550901, for supporting the development of ASPECT. Computations were  
 277 performed on Beijing Super Cloud Computing Center.

## 278 Open Research

279 The code (ASPECT v2.3.0, Wolfgang et al., 2021) used in this study is available at  
 280 <https://doi.org/10.5281/zenodo.5131909>.

## 281 References

- 282 Agard, P., Jolivet, L., Vrielynck, B., Burov, E., Monie, P., 2007. Plate acceleration: the obduction trigger? *Earth*  
 283 *Planet. Sci. Lett.* 258, 428–441. <https://doi.org/10.1016/j.epsl.2007.04.002>
- 284 Agard, P., Yamato, P., Soret, M., Prigent, C., Guillot, S., Plunder, A., Dubacq, B., Chauvet, A., Monie, P., 2016.  
 285 Plate interface rheological switches during subduction infancy: control on slab penetration and metamorphic  
 286 sole formation. *Earth Planet. Sci. Lett.* 451, 208–220. <https://doi.org/10.1016/j.epsl.2016.06.054>
- 287 Almeida, J., Riel, N., Rosas, F. M., Duarte, J. C., & Kaus, B. (2022). Self-replicating subduction zone initiation by  
 288 polarity reversal. *Communications Earth & Environment*, 3(1), 55. <https://doi.org/10.1038/s43247-022-00380-2>
- 289 Bangerth, W., Dannberg, J., Gassmoeller, R., & Heister, T. 2020. ASPECT v2.2.0. (version v2.2.0). Zenodo.  
 290 <https://doi.org/10.5281/ZENODO.3924604>
- 291 Bercovici, D., 2003. The generation of plate tectonics from mantle convection. *Earth Planet. Sci. Lett.* 205, 107–  
 292 121. [https://doi.org/10.1016/S0012-821X\(02\)01009-9](https://doi.org/10.1016/S0012-821X(02)01009-9)
- 293 Dong, M., Lü, C.C., Zhang, J., & Hao, T., 2022. Downgoing plate-buoyancy driven retreat of North Sulawesi  
 294 Trench: Transition of a passive margin into a subduction zone. *Geophys. Res. Lett.* 49, e2022GL101130.  
 295 <https://doi.org/10.1029/2022GL101130>
- 296 Gerya, T., Stern, R.J., Baes, M., Sobolev, S., Whattam, S., 2015. Plume-induced subduction initiation triggered plate  
 297 tectonics on Earth. *Nature* 527, 221–225. <https://doi.org/10.1038/nature15752>
- 298 Gurnis, M., Hall, C., Lavier, L., 2004. Evolving force balance during incipient subduction. *Geochem. Geophys.*  
 299 *Geosyst.* 5, Q07001. <http://dx.doi.org/10.1029/2003GC000681>
- 300 Hall, C. E., Gurnis, M., Sdrolias, M., Lavier, L. L., Müller, R. D., 2003. Catastrophic initiation of subduction  
 301 following forced convergence across fracture zones. *Earth Planet. Sci. Lett.* 212, 15–30.  
 302 [https://doi.org/10.1016/S0012-821X\(03\)00242-5](https://doi.org/10.1016/S0012-821X(03)00242-5)
- 303 Hall, R., 1996. Reconstructing cenozoic SE Asia. *Geol. Soc. Lond., Spec. Publ.* 106, 153–184.  
 304 <https://doi.org/10.1144/gsl.sp.1996.106.01.11>
- 305 Hall, R., 2012. Late Jurassic–Cenozoic reconstructions of the Indonesian region and the Indian Ocean,  
 306 *Tectonophysics*, 570–571, 1–41. <https://doi.org/10.1016/j.tecto.2012.04.021>
- 307 Hall, R., 2019. The subduction initiation stage of the Wilson cycle, *Geological Society, London, Special*  
 308 *Publications*, 470(1), 415–437. <https://doi.org/10.1144/SP470.3>
- 309 Hall, R. & Spakman, W., 2015. Mantle structure and tectonic history of SE Asia. *Tectonophysics* 658, 14–45.  
 310 <https://doi.org/10.1016/j.tecto.2015.07.003>
- 311 Hayes, G. P., Moore, G. L., Portner, D. E., Hearne, M., Flamme, H., Furtney, M., & Smoczyk, G. M., 2018. Slab2, a  
 312 comprehensive subduction zone geometry model, *Science*, 362(6410), 58–61.  
 313 <https://doi.org/10.1126/science.aat4723>
- 314 Heister, T., Dannberg, J., Gassmüller, R., & Bangerth, W., 2017. High Accuracy Mantle Convection Simulation  
 315 through Modern Numerical Methods-II: Realistic Models and Problem. *Geophysical Journal International*, 210,  
 316 833–851. <https://doi.org/10.1093/gji/ggx195>
- 317 Husson, L., Riel, N., Aribowo, S., Authemayou, C., de Gelder, G., Kaus, B. J. P., Mallard, C., Natawidjaja, D. H.,  
 318 Pedoja, K. & Sarr, A. C. (2022). Slow geodynamics and fast morphotectonics in the far East Tethys.  
 319 *Geochemistry, Geophysics, Geosystems*, 23(1), e2021GC010167. <https://doi.org/10.1029/2021GC010167>
- 320 Ishizuka, O., Tani, K., Reagan, M. K., Kanayama, K., Umino, S., Harigane, Y., Sakamoto, I., Miyajima, Y., Yuasa,  
 321 M., Dunkley, D. J., 2011. The timescales of subduction initiation and subsequent evolution of an oceanic island  
 322 arc. *Earth Planet. Sci. Lett.* 306(3–4), 229–240. <https://doi.org/10.1016/j.epsl.2011.04.006>

- 323 Kopp, C., Flueh, E. R., & Neben, S., 1999. Rupture and accretion of the Celebes Sea crust related to the North  
 324 Sulawesi subduction combined interpretation of reflection and refraction seismic measurements. *Journal of*  
 325 *Geodynamics*, 27(3), 309-325. [https://doi.org/10.1016/S0264-3707\(98\)00004-0](https://doi.org/10.1016/S0264-3707(98)00004-0)
- 326 Korenaga, J., 2012. Plate tectonics and planetary habitability: current status and future challenges. *Ann. N.Y. Acad.*  
 327 *Sci.* 1260, 87-94. <https://doi.org/10.1111/j.1749-6632.2011.06276.x>
- 328 Korenaga, J., 2013. Initiation and evolution of plate tectonics on Earth: theories and observations. *Annu. Rev. Earth*  
 329 *Planet. Sci.* 41, 117–151. <https://doi.org/10.1146/annurev-earth-050212-124208>
- 330 Kronbichler, M., Heister, T., & Bangerth, W., 2012. High Accuracy Mantle Convection Simulation through Modern  
 331 Numerical Methods. *Geophysical Journal International*, 191, 12–29. <https://doi.org/10.1111/j.1365-246X.2012.05609.x>
- 332  
 333 Lai, C.-K., Xia, X.-P., Hall, R., Meffre, S., Tsikouras, B., Rosana Balangué Tarriela, M. I., et al., 2021. Cenozoic  
 334 evolution of the Sulu Sea arc-basin system: An overview. *Tectonics*, 40, e2020TC006630.  
 335 <https://doi.org/10.1029/2020TC006630>
- 336 Leng, W., & Gurnis, M., 2015. Subduction initiation at relic arcs. *Geophys. Res. Lett.* 42(17), 7014-7021.  
 337 <https://doi.org/10.1002/2015gl064985>
- 338 Li M, Huang S, Hao T, Dong M, Xu Y, Zhang J, He Q, Fang G., 2023. Neogene subduction initiation models in the  
 339 western Pacific and analysis of subduction zone parameters. *Science China Earth Sciences*, 66(3): 472–491,  
 340 <https://doi.org/10.1007/s11430-022-1065-1>
- 341 Marques, F. O., Nikolaeva, K., Assumpção, M., Gerya, T. V., Bezerra, F. H. R., do Nascimento, A. F., & Ferreira, J.  
 342 M., 2013. Testing the influence of far-field topographic forcing on subduction initiation at a passive margin.  
 343 *Tectonophysics*, 608, 517-524. <https://doi.org/10.1016/j.tecto.2013.08.035>
- 344 Marques, F. O., Cabral, F. R., Gerya, T. V., Zhu, G. & May, D. A., 2014. Subduction initiates at straight passive  
 345 margins. *Geology*, 42, 331-334. <https://doi.org/10.1130/G35246.1>
- 346 Maunder B, Prytulak J, Goes S, et al. Rapid subduction initiation and magmatism in the Western Pacific driven by  
 347 internal vertical forces. *Nature Communications*, 2020, 11: 1874. <https://doi.org/10.1038/s41467-020-15737-4>
- 348 McKenzie, D.P., 1977. The initiation of trenches: a finite amplitude instability. In: Talwani, M., Pittman, W.C.  
 349 (Eds.), *Island Arcs, Deep Sea Trenches, and Back-Arc Basins*. Maurice Ewing Ser. I. AGU, Washington, D.C.,  
 350 pp. 57–61.
- 351 Mueller, S., Phillips, R.J., 1991. On the initiation of subduction. *J. Geophys. Res.* 96, 651–665.
- 352 Nikolaeva, K., Gerya, T. V., Marques, F. O., 2010. Subduction initiation at passive margins: Numerical modeling. *J.*  
 353 *Geophys. Res.* 115, B03406. <https://doi.org/10.1029/2009JB006549>
- 354 Nikolaeva, K., Gerya, T. V., Marques, F. O., 2011. Numerical analysis of subduction initiation risk along the  
 355 Atlantic American passive margins. *Geology* 39, 463-466. <https://doi.org/10.1130/G31972.1>
- 356 Niu, Y., O'HARA, M. J., Pearce, J. A., 2003. Initiation of subduction zones as a consequence of lateral  
 357 compositional buoyancy contrast within the lithosphere: a petrological perspective. *Journal of Petrology*, 44(5),  
 358 851-866. <https://doi.org/10.1093/petrology/44.5.851>
- 359 Riel, N., Duarte, J. C., Almeida, J., Kaus, B. J., Rosas, F., Rojas-Agramonte, Y., & Popov, A. (2023). Subduction  
 360 initiation triggered the Caribbean large igneous province. *Nat Commun* 14, 786 (2023).  
 361 <https://doi.org/10.1038/s41467-023-36419-x>
- 362 Rudyawan, A., & Hall, R. (2012). Structural reassessment of the South Banggai-Sula area: no Sorong fault zone. In:  
 363 *Proceedings of the Indonesian Petroleum Association, 36th Annual Convention, Indonesian Petroleum*  
 364 *Association, Jakarta, Indonesia, IPA12-G-030* 1–17.
- 365 Sandwell, D. T., Smith, W. H. F., 2009. Global marine gravity from retracked Geosat and ERS-1 altimetry: Ridge  
 366 Segmentation versus spreading rate. *J. Geophys. Res. Atmosphere*, 114(B1): B01411.  
 367 <https://doi.org/10.1029/2008JB006008>
- 368 Schlüter, H. U., Block, M., Hinz, K., Neben, S., Seidel, D., & Djajadihardja, Y., 2001. Neogene sediment thickness  
 369 and Miocene basin-floor fan systems of the Celebes Sea. *Marine and petroleum geology*, 18(7), 849-861.  
 370 [https://doi.org/10.1016/S0264-8172\(01\)00027-7](https://doi.org/10.1016/S0264-8172(01)00027-7)
- 371 Seton, M., Müller, R. D., Zahirovic, S., Williams, S., Wright, N. M., Cannon, J., Whittaker, J. M., Matthews, K. J.,  
 372 & McGirr, R. (2020). A global data set of present-day oceanic crustal age and seafloor spreading parameters.  
 373 *Geochemistry, Geophysics, Geosystems*, 21(10), e2020GC009214. <https://doi.org/10.1029/2020GC009214>
- 374 Shuck, B., Gulick, S.P.S., Van Avendonk, H.J.A. et al., 2022. Stress transition from horizontal to vertical forces  
 375 during subduction initiation. *Nat. Geosci.* 15, 149–155. <https://doi.org/10.1038/s41561-021-00880-4>
- 376 Silver, E. A., Mccaffrey, R., Smith, R. B., 1983. Collision, Rotation, and the Initiation of Subduction in the  
 377 Evolution of Sulawesi, Indonesia. *J. Geophys. Res.* 88, 9407-9418. <https://doi.org/10.1029/JB088iB11p09407>
- 378 Stern, R. J., 2004. Subduction initiation: spontaneous and induced, *Earth Planet. Sci. Lett.*, 226(3-4), 275-292.

- 379 [https://doi.org/10.1016/s0012-821x\(04\)00498-4](https://doi.org/10.1016/s0012-821x(04)00498-4)  
380 Stern, R. J., Gerya, T., 2018. Subduction initiation in nature and models: A review, *Tectonophysics*, 746, 173-198.  
381 <https://doi.org/10.1016/j.tecto.2017.10.014>  
382 Toth, J., Gurnis, M., 1998. Dynamics of subduction initiation at preexisting fault zones. *J. Geophys. Res. Solid*  
383 *Earth*, 103(B): 18053-18067. <https://doi.org/10.1029/98JB01076>  
384 Turcotte, D. L., & Schubert, G., 2014. *Geodynamics*. Cambridge, UK: Cambridge University Press.  
385 Wolfgang Bangerth, Juliane Dannberg, Menno Fraters, Rene Gassmoeller, Anne Glerum, Timo Heister, & John  
386 Naliboff. (2021). ASPECT v2.3.0 (v2.3.0). Zenodo. <https://doi.org/10.5281/zenodo.5131909>  
387 Zhou, X., Li, Z. H., Gerya, T. V., Stern, R. J., 2020. Lateral propagation-induced subduction initiation at passive  
388 continental margins controlled by preexisting lithospheric weakness. *Sci. Adv.*, 6, eaaz1048.  
389 <https://doi.org/10.1126/sciadv.aaz1048>  
390 Zhou, X., Li, Z. H., Gerya, T. V., Stern, R. J., Xu Z., Zhang J., 2018. Subduction initiation dynamics along a  
391 transform fault control trench curvature and ophiolite ages. *Geology*, 46(7), 607-610.  
392 <https://doi.org/10.1130/G40154.1>

### 393 **References From the Supporting Information**

- 394 Hirth, G. & Kohlstedt, D., 2003. Rheology of the upper mantle and the mantle wedge: a view from the  
395 experimentalists. in *Inside the Subduction Factory* (ed. Eiler, J.) Vol. 183 of *Geophysical Monograph*  
396 (American Geophysical Union)  
397 Gleason, G. C., & Tullis, J., 1995. A flow law for dislocation creep of quartz aggregates determined with the molten  
398 salt cell. *Tectonophysics*, 247(1-4), 1-23. [https://doi.org/10.1016/0040-1951\(95\)00011-B](https://doi.org/10.1016/0040-1951(95)00011-B)  
399 Glerum, A. C., Thieulot, C., Fraters, M., Blom, C., Spakman, W., 2018. Nonlinear viscoplasticity in ASPECT:  
400 benchmarking and applications to subduction. *Solid Earth* 9, 267–294. <https://doi.org/10.5194/se-9-267-2018>  
401 Wilks, K. R., & Carter, N. L., 1990. Rheology of some continental lower crustal rocks. *Tectonophysics*, 182(1-2),  
402 57-77. [https://doi.org/10.1016/0040-1951\(90\)90342-6](https://doi.org/10.1016/0040-1951(90)90342-6)  
403 Ranalli, 1995. *Rheology of the Earth*. 2nd ed. London: Chapman & Hall.  
404 Rybacki, E., Gottschalk, M., Wirth, R., Dresen, G., 2006. Influence of water fugacity and activation volume on the  
405 flow properties of fine-grained anorthite aggregates. *J. Geophys. Res. Solid Earth*, 111, 3663.  
406 <https://doi.org/10.1029/2005JB003663>  
407

408 **Figure 1.** (a) Oceanic basins and subduction zones in Southeast Asia. The ages of the oceanic  
409 basins are taken from Seton et al. (2020). NBS indicates the North Banda Sea, and SBS indicates  
410 the South Banda Sea. (b) Bathymetric image of the North Banda Sea and surrounding regions,  
411 taken from Fig. 7 in Hall (2019). (c) Subducted Celebes Sea Plate in the North Sulawesi and  
412 Cotabato trenches (the gray irregular polygons indicate the shape of the subducting plate  
413 projected onto the surface, while the red irregular polygons are reconstructions of the subducted  
414 plate). (d) Diagram of subducted plate reconstruction to the surface. The black line represents the  
415 subducted slab. The calculated length is shown on the surface as a red line. The slab dip along  
416 the C–D profile was not certain from earthquake events and was extracted from the Slab2 model  
417 (Hayes et al., 2018).

418 **Figure 2.** (a) Initial stage showing the triangular indenter structure to simulate curved margins,  
419 the base length of the indenter ( $D$ ), and the angle of the indenter ( $\alpha$ ). A zoom-in of the  
420 computational mesh shows that the minimum resolution is  $\sim 3$  km. (b) Plate strength and density  
421 contrast between the oceanic and overriding plates. (c) Indenter geometries in different model  
422 experiments.

423 **Figure 3.** (a) Final results of Models 0–3 showing only the oceanic crust and suboceanic  
424 lithospheric mantle. Models 1–3 have the same  $D$  (200 km) and different angles ( $\alpha$ ). (b) Sections  
425 through end results (at 3.2 Myr) for Model 2 at  $y = 0$  km (front),  $y = 200$  km (middle), and  $y =$   
426 400 km (back). The oceanic slab reaches a depth of 200 km faster in the middle than in the front  
427 and back. The colors indicate the composition, as defined in Figure 2a.

428 **Figure 4.** Sections through models at  $z = 0$  km. (a) Shear stresses ( $\tau_{xy}$ ) on the surfaces of Models  
429 1, 2, and 3 at the initial stage. (b) Evolution of the indenter geometry. The dashed lines represent  
430 the lengths of  $D$  and  $h$  in the initial stage.  $\Delta h$  represents the decrease in the length of  $h$ . The black  
431 arrows indicate the velocity.

Figure 1.

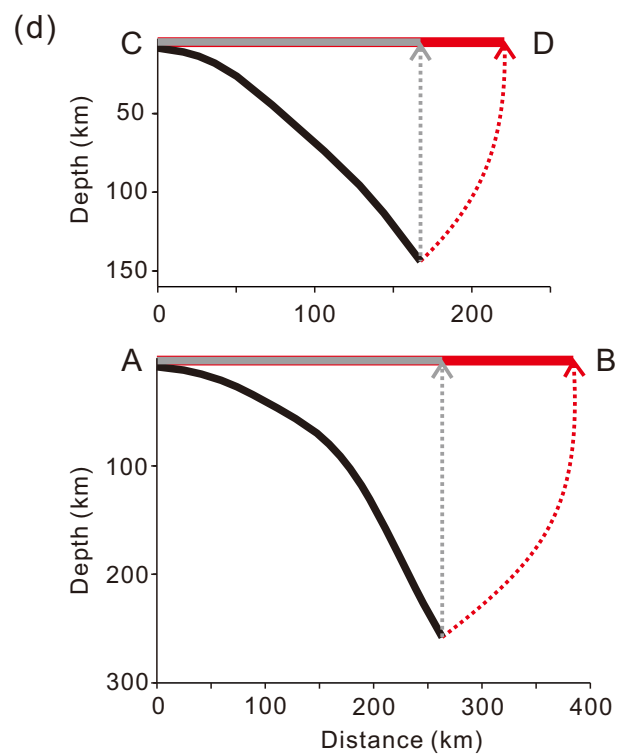
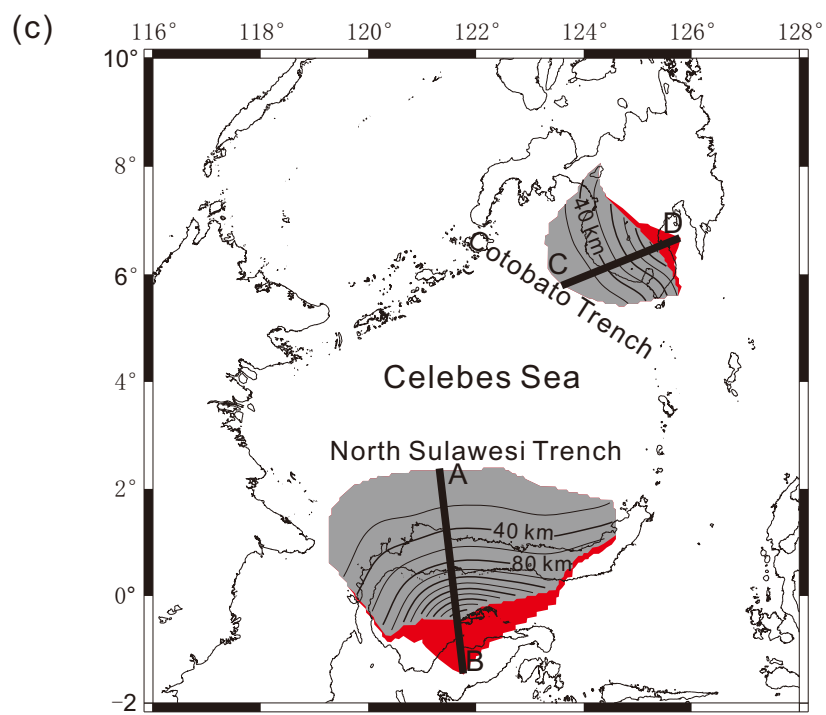
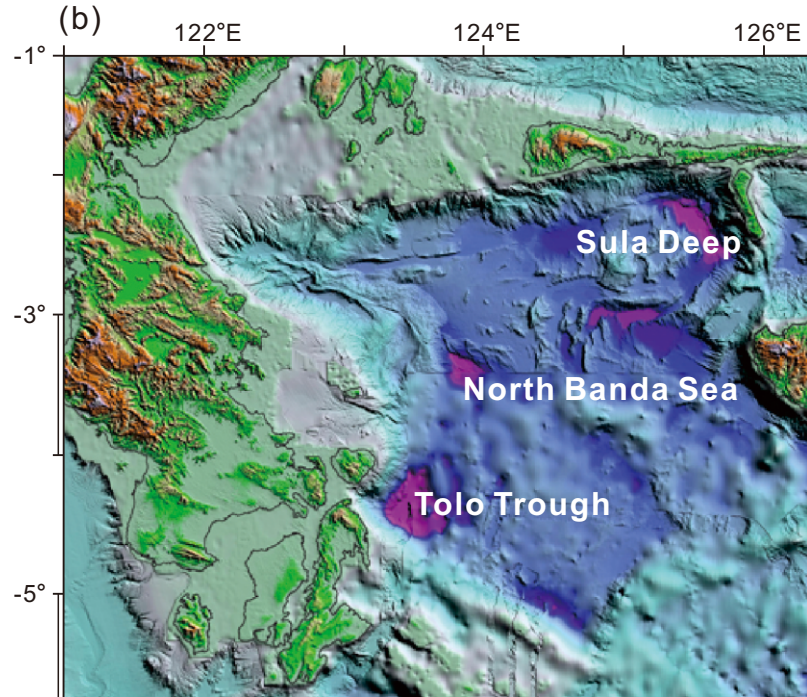
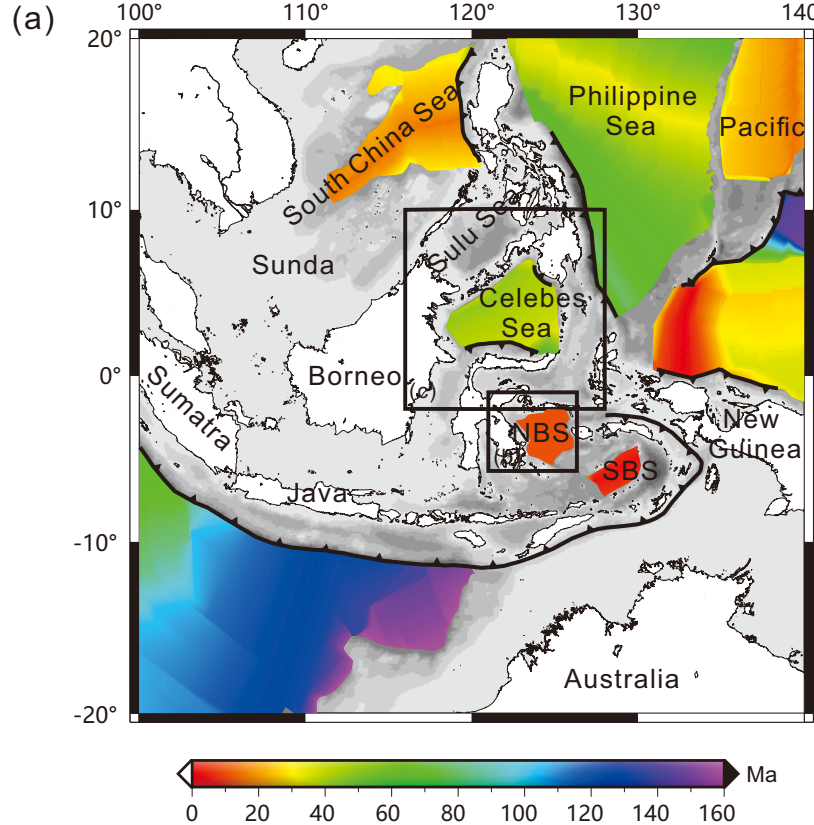


Figure 2.

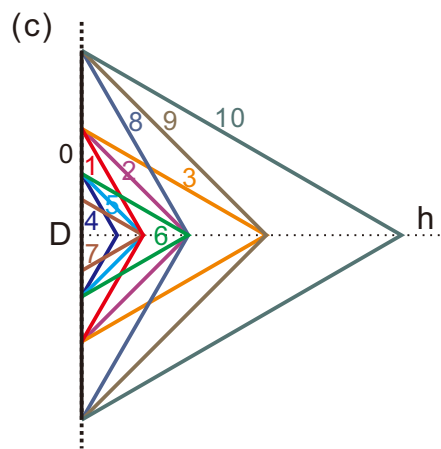
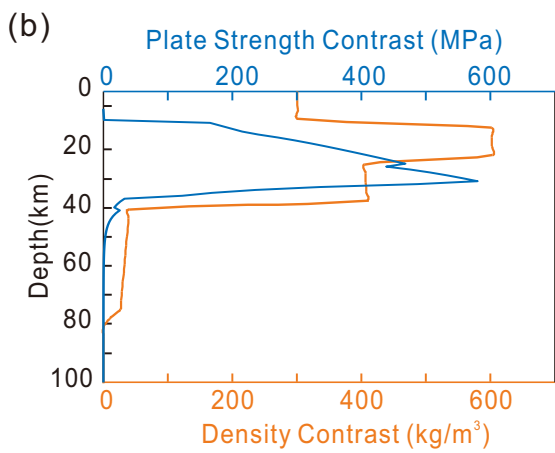
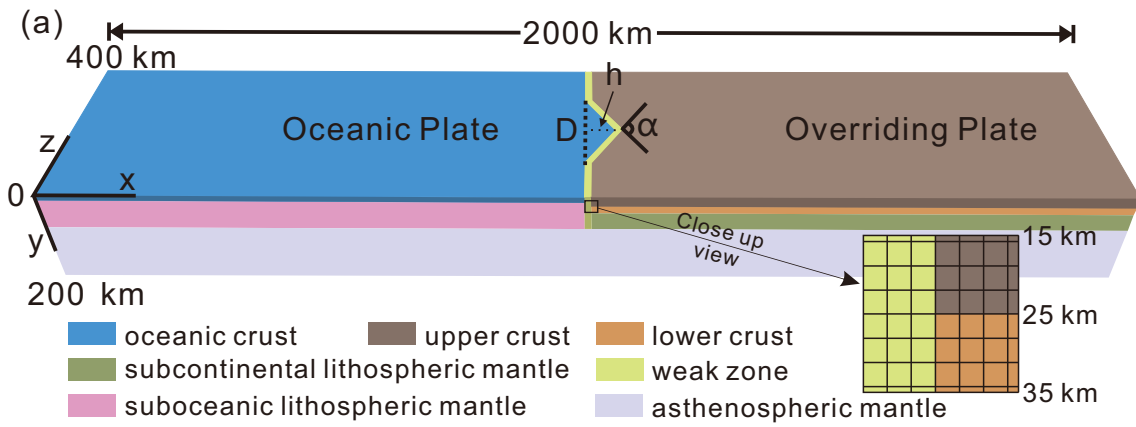


Figure 3.

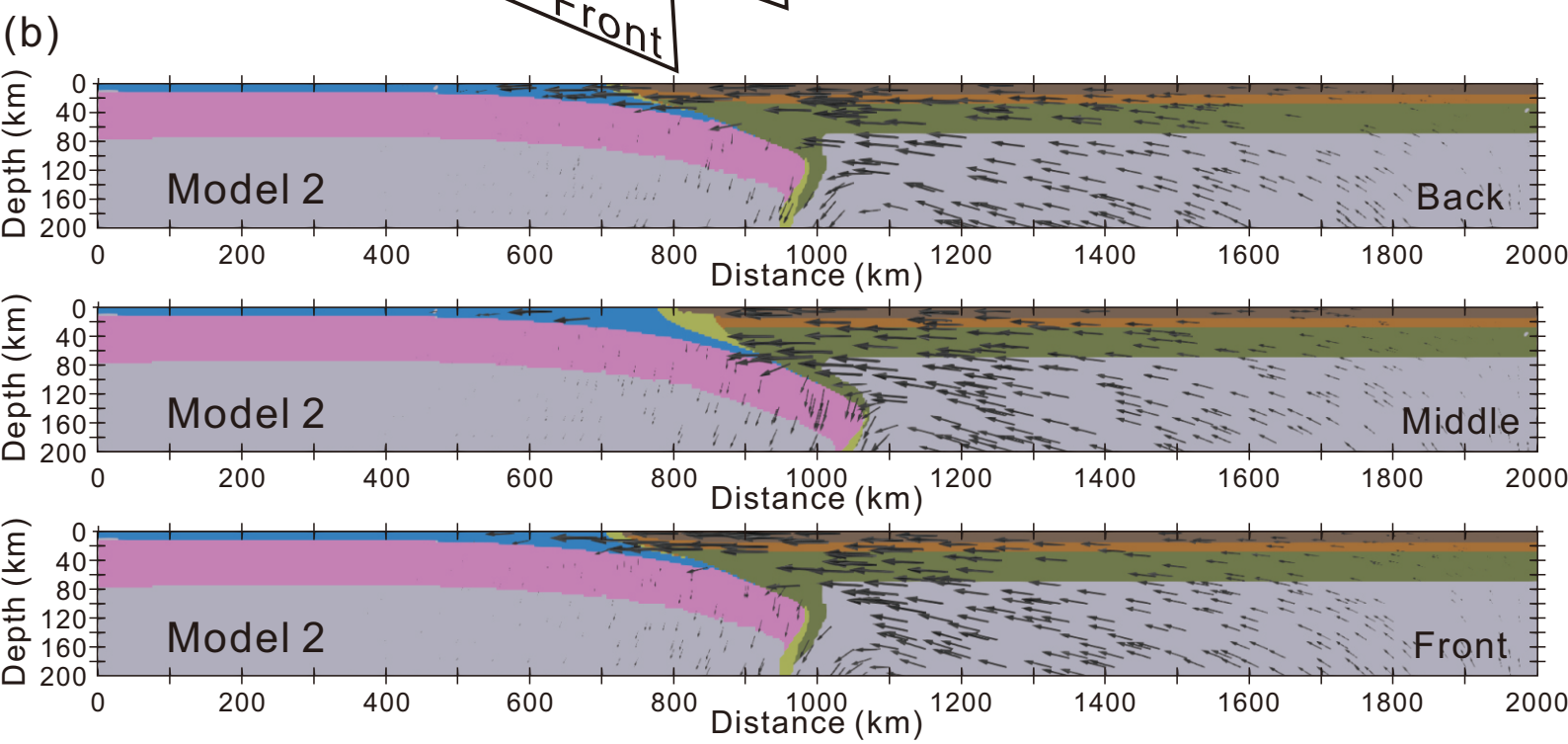
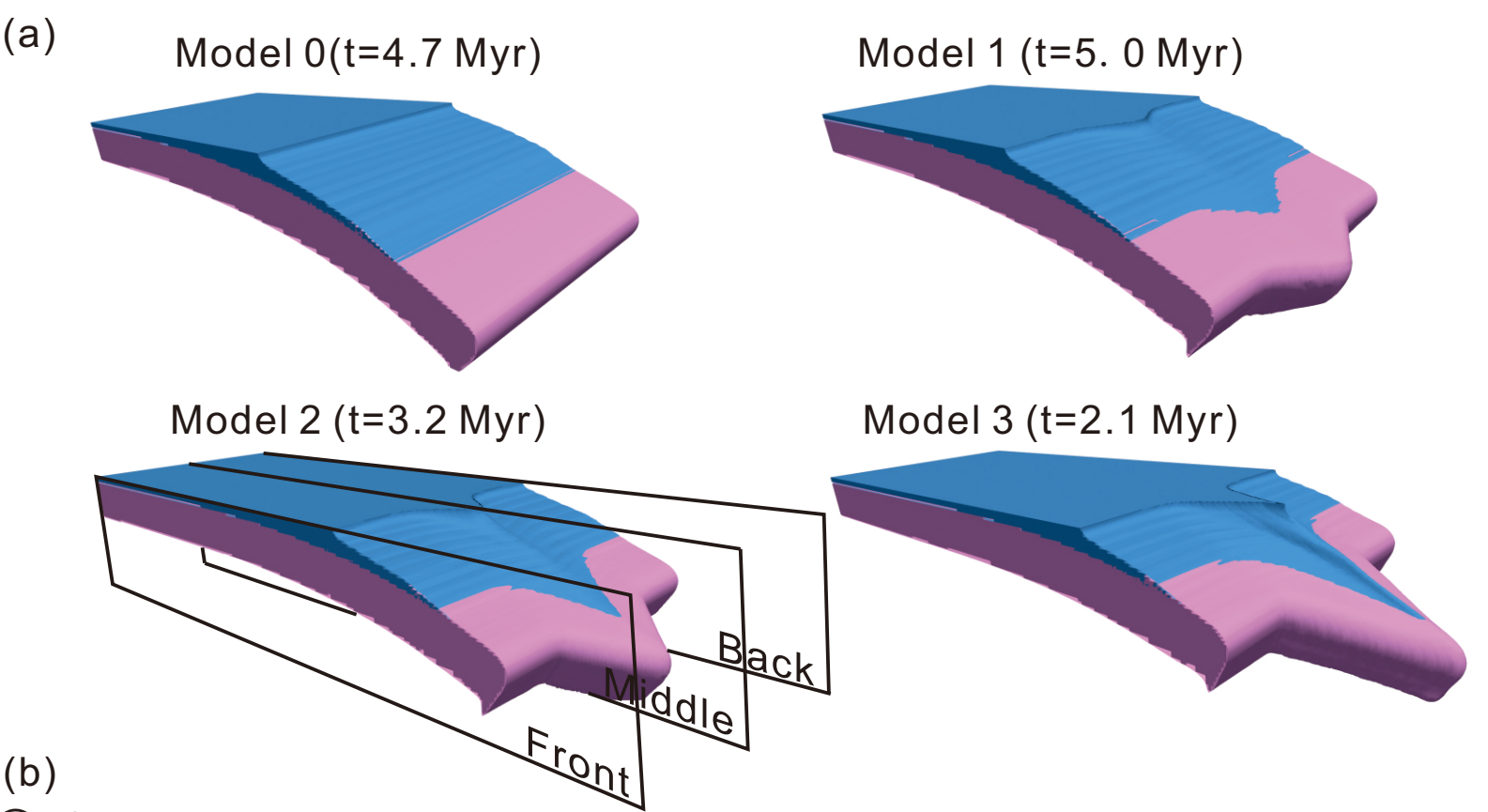
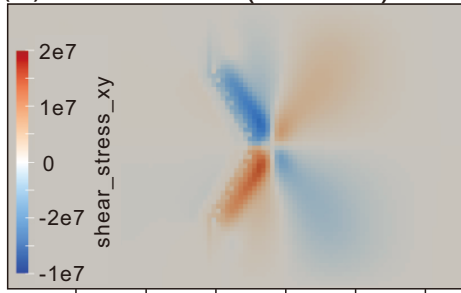
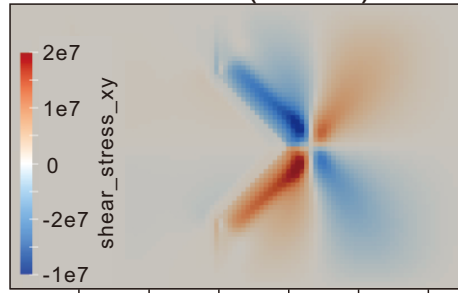


Figure 4.

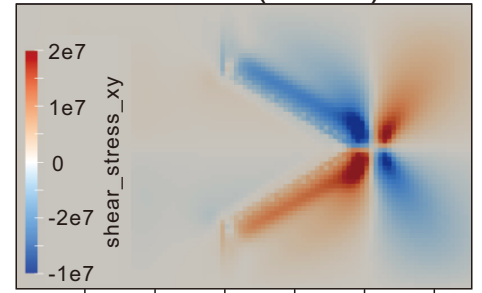
(a) Model 1 ( $\alpha=120^\circ$ )



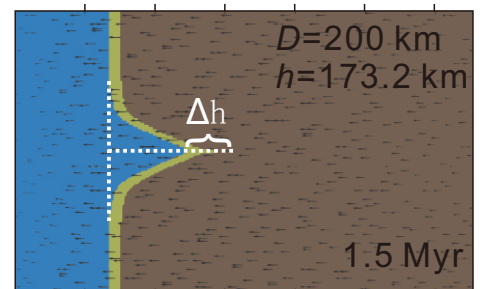
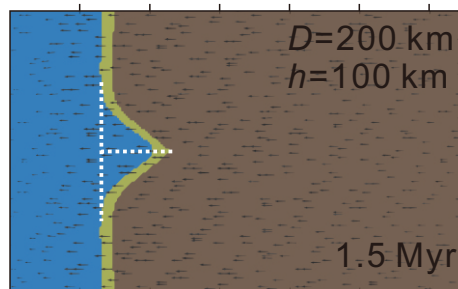
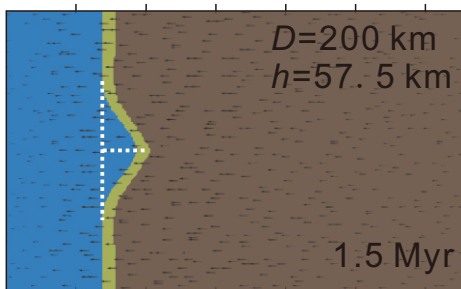
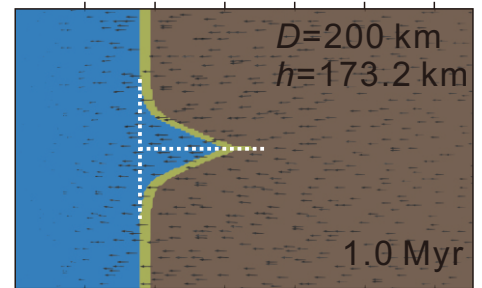
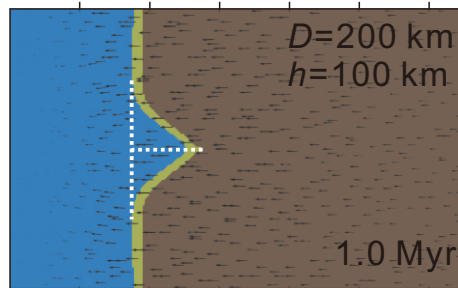
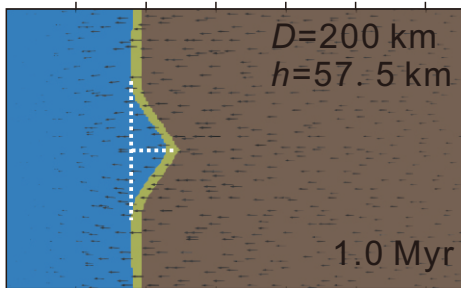
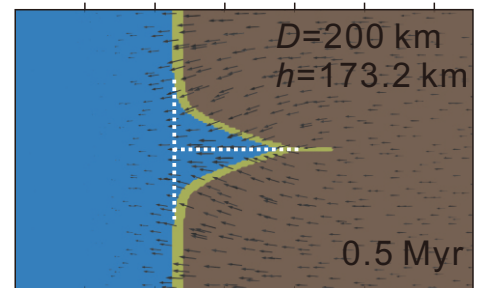
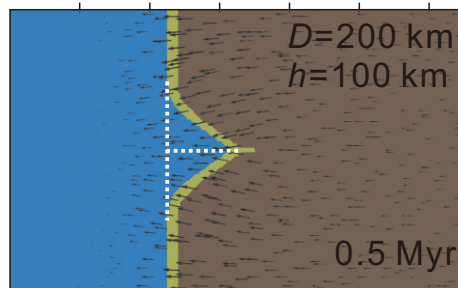
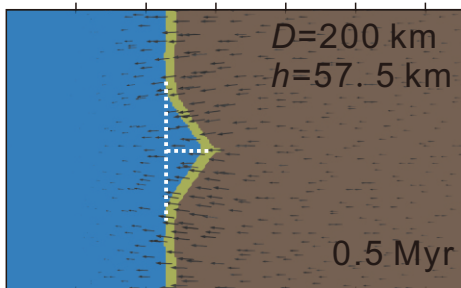
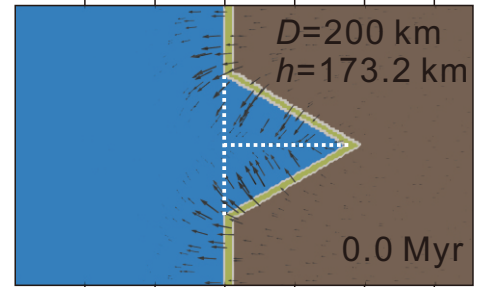
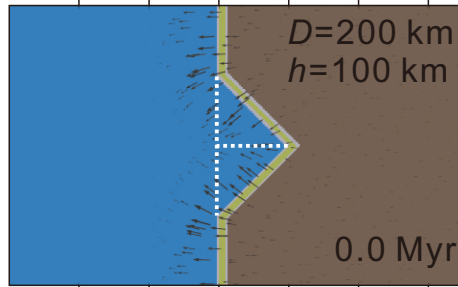
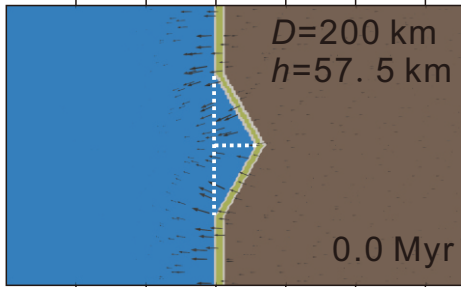
Model 2 ( $\alpha=90^\circ$ )



Model 3 ( $\alpha=60^\circ$ )



(b)



800 1000 1200

800 1000 1200

800 1000 1200

**Table 1.** Description of numerical experiments with varying length and angle of the indenter

Model	$D$ (km)	$\alpha$ ( $^{\circ}$ )	$h$ (km)	Time of subduction initiation $\pm 0.1$ (Myr)
0	0	180	0	4.7
1	200	120	57.7	5.0
2	200	90	100	3.2
3	200	60	173.2	2.2
4	115.4	120	33.3	4.8
5	115.4	90	57.7	4.2
6	115.4	60	100	2.8
7	66.6	60	57.7	3.6
8	346.4	120	100	4.5
9	346.4	90	173.2	4.3
10	346.4	60	300	2.4